PERGAMON

PII: S1359-6454(99)00023-3

MICROMECHANICS MODEL FOR THE DETACHMENT OF RESIDUALLY COMPRESSED BRITTLE FILMS AND COATINGS

A. G. EVANS[1], J. W. HUTCHINSON[1]† and M. Y. HE[2]

[1]Division of Engineering and Applied Sciences, Harvard University, Cambridge, MA 02138, U.S.A. and
[2]Materials, University of California, Santa Barbara, CA 93106, U.S.A.

Abstract—The durability of residually compressed coatings, particularly thermal barrier coatings (TBCs), is governed by events occurring at the interface with the substrate. In general, failure involves the sequential nucleation growth and coalescence of separations in the presence of imperfections and defects. The growth and coalescence phases are analyzed. Remnant ligaments are expected from the mechanics. These allow the coating to remain attached to the substrate, even when interface separation is profuse. Detachment happens when transverse loads develop. Critical values of these loads are calculated and their implications discussed. © 1999 Acta Metallurgica Inc. Published by Elsevier Science Ltd. All rights reserved.

1. INTRODUCTION

The integrity of relatively thick, brittle coatings attached to metal substrates has emerged as an increasingly important consideration, as such coatings become more widely implemented. Thermal barrier coatings (TBCs) typify the applications [1–5]. These coating systems often need to retain their integrity when subject to thermal cycling through large temperature ranges, despite significant thermal expansion misfit with the substrate. Accordingly, they are designed to have high in-plane compliance. This is achieved by deliberately incorporating either aligned porosity or microcrack arrays. These methods for incorporating compliance also result in low strength and toughness. Yet, the systems have high durability (often remarkably so). Eventually, the coating spalls away and exposes the substrate. One engineering problem is that the time/cycles to failure exhibits large variability. Understanding and reducing this variability would constitute a major benefit to the expanded and more confident implementation of coatings. This article addresses some aspects of this problem.

A micromechanics approach is taken, based on mechanisms of crack nucleation, growth and coalescence. It is illustrated for TBCs, wherein the energy density needed to induce failure is provided by a thermally grown oxide (referred to as TGO: typically α-alumina) that forms between the TBC and the substrate (usually a Ni- or Pi-based bond coat alloy) [6–9]. The TGO is subject to large compressive stress caused primarily by thermal expansion misfit with the substrate (there are additional growth stresses in some cases). The redistribution of these stresses by morphological imperfections in the TGO, and by other defects [10–22], provides the energy release rate needed to extend and coalesce the separations that cause failure.

Interfacial micro-separations develop from imperfections in the coating (with time/cycles) and become extensive enough to cover an appreciable fraction of the cross-section prior to failure. The coalescence of a domain of such separations into a crack comprises the penultimate phase in the failure sequence. It precedes edge or buckle driven delamination [13, 14]. When large enough, the delamination detaches the coating. This happens when the associated energy release rate exceeds the remnant toughness of the degraded domain.

Solutions to this failure category are provided at several levels of simplification that could lead, ultimately, to a stochastic life prediction model. The most basic model comprises a domain of included imperfections located along a weak plane, subject to a misfit stress in an otherwise isotropic, elastically homogeneous solid [Fig. 1(a)]. Results for this problem can be obtained analytically and provide a basic comprehension of the principles. At a more representative level for coatings, a numerical analysis is performed for an idealized TBC system comprising an electron beam physical vapor deposited (EB-PVD) thermal barrier on a bond coat, with a TGO containing a periodic array of imperfections [Fig. 1(b)]. A single example is used to demonstrate the important issues.

The article is organized as follows. In Section 2, the concepts are outlined. In Section 3, analytical results for the coalescence of separations between heterogeneities are presented. In Sections 4 and 5,

---

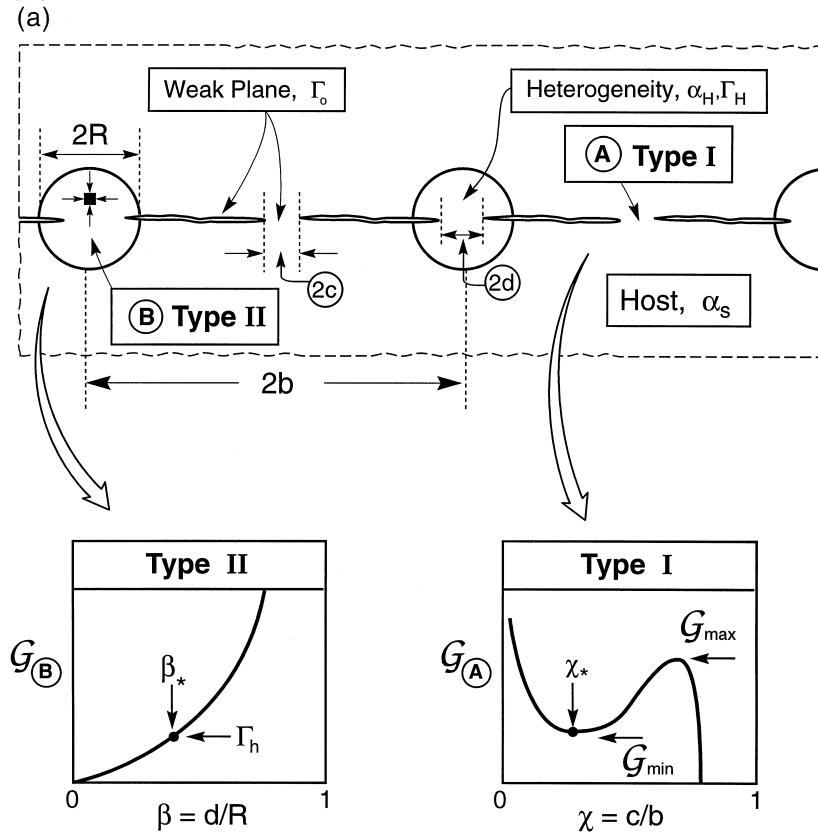†To whom all correspondence should be addressed.

(a)

Fig. 1. The two models used to analyze the phases of crack coalescence: (a) inclusion model; (b) film model. The type I and II ligaments are identified, as well as the expected energy release rate trends as the ligaments converge.

remnant ligaments within heterogeneities and their detachment to cause failure are analyzed, analytically. In Section 6, a numerical example for a coating is presented. Finally, in Section 7, the implications for delamination are discussed.

2. THE BASIC CONCEPT

Considerations of crack coalescence from an array of heterogeneities subject to misfit strain (Fig. 1) provide two fundamental mechanics precepts, both associated with the convergence of cracks in residually stressed systems. The concepts are introduced for the case of an elastically homogeneous body containing a periodic co-linear array of cylindrical imperfections having lower thermal expansion coefficient (α_H) than the surrounding host (α_s). The imperfections are connected by a weak plane. Microseparations form on that plane and converge, resulting in intact ligaments (Fig. 1). There are two types of ligament: those *between* imperfections (type I) and those *within* the imperfections (type II). Type I ligaments experience residual tensions. The energy release rate (at location A in Fig. 1) has the form depicted on the inset as G_A. Namely, it becomes unbounded as the separations

converge, resulting in a minimum G_{min} at ligament size c_*. Once the ligament diminishes to c_* (by time/cycle dependent growth) the separations abruptly coalesce.

The situation is completely different at type II ligaments within the imperfections (location B in Fig. 1), which experience residual compression. Now, because the residually stressed regions diminish to zero as ligaments coalesce, the energy release rate tends to zero, as indicated by the inset. Accordingly, for a periodic array of imperfections, *small ligaments, length d_c, always stay attached.* This is the converging debond situation elaborated elsewhere for films and fiber composites [15–17]. The most vivid visualization has been provided for debonded thin films (Fig. 2).

The remnant ligaments can be detached when other loading situations arise, such as the application of a mechanical load or when moderately large delaminations are present. One illustration is depicted in Fig. 3, comprising attached ligaments ahead of an edge delamination. Now, the displacements associated with the crack faces provide a different loading environment, wherein the energy release rate becomes unbounded as the remnant ligament size tends to zero, $d \longrightarrow 0$. This process is characterized by a strength and a fracture toughness
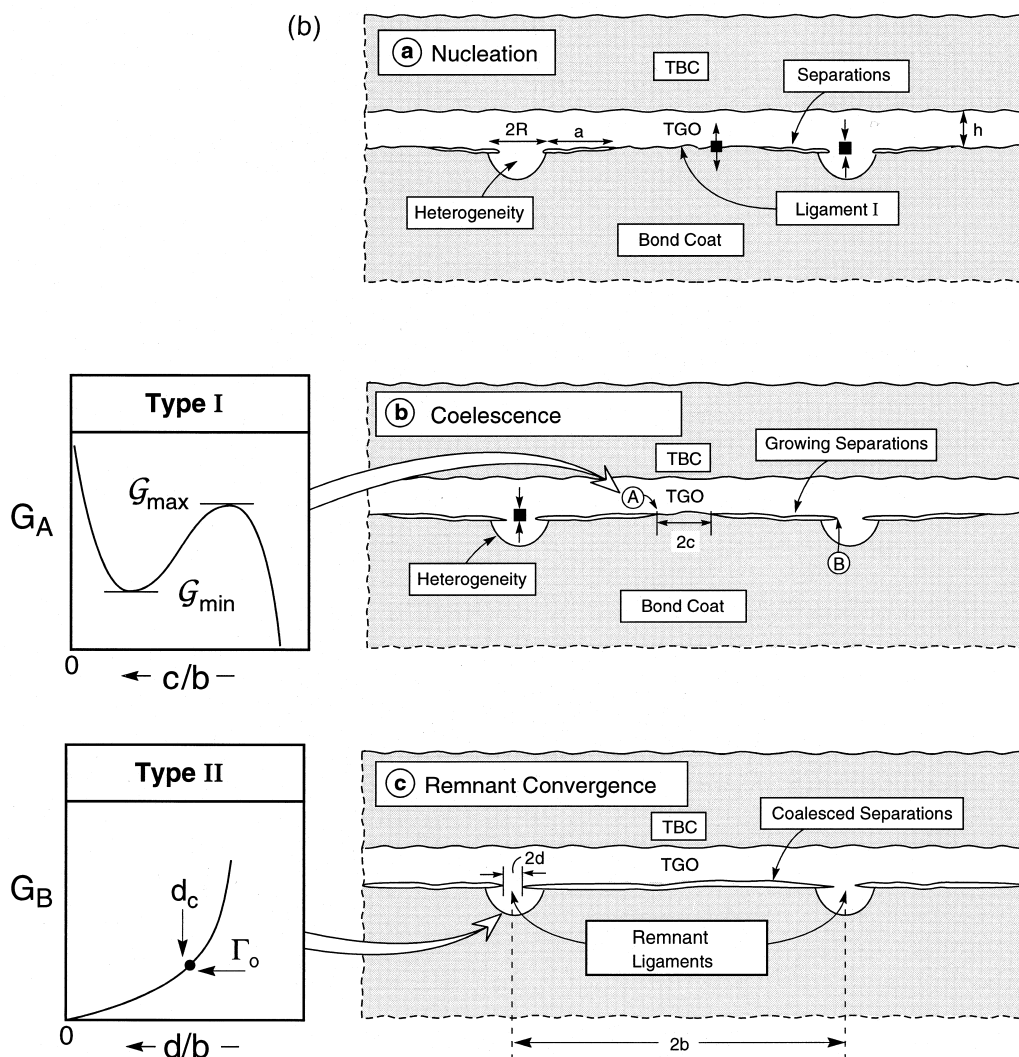
Fig. 1. *continued*

for the plane held together by the ligaments. The criterion that governs failure of attached type II ligaments establishes life. These three phases of the failure sequence are explored below.

The problem has similarities with crack evolution from other centers of dilatation, such as indentations and inclusions [18, 19]. Analytical results that provide useful non-dimensional groups and approximate trends connect with this prior work. The results are presented either in terms of stress intensity factors, K, or energy release rates, G, which can be interrelated in the usual way: $K = \sqrt{\bar{E}G}$, with $\bar{E}$ the bimaterial plane strain modulus (i.e. $\bar{E} = E/(1 - v^2)$ for the limit of no mismatch).

The presence of remnant ligaments and their detachment upon application of transverse stresses has been experimentally demonstrated in a recent study of failure mechanisms in thermal barrier coatings [20]. The findings of this assessment indicate that inter-heterogeneity coalescence along the TGO/substrate interface occurs with relative facility (Fig. 4). Conversely, the intra-heterogeneity ligaments remain intact until a wedge impression is used to impose transverse stresses. These additional stresses rupture the attached ligaments, which remain embedded in the substrate (Fig. 4).

3. LIGAMENT COALESCENCE

For determination of the qualitative trend in the relationships pertinent to the coalescence of type I ligaments, a two-dimensional plane strain model is employed. The model uses results for an infinite co-linear array of cracks in an infinite homogeneous solid. The cracks are equally spaced a distance $2b$, center-to-center, and separated by ligaments of length $2c$ [cf. Fig. 1(a)]. No attempt is made to replicate the details of the pressure distribution exerted by the imperfection on the crack faces. Instead, an approximation is obtained by taking a
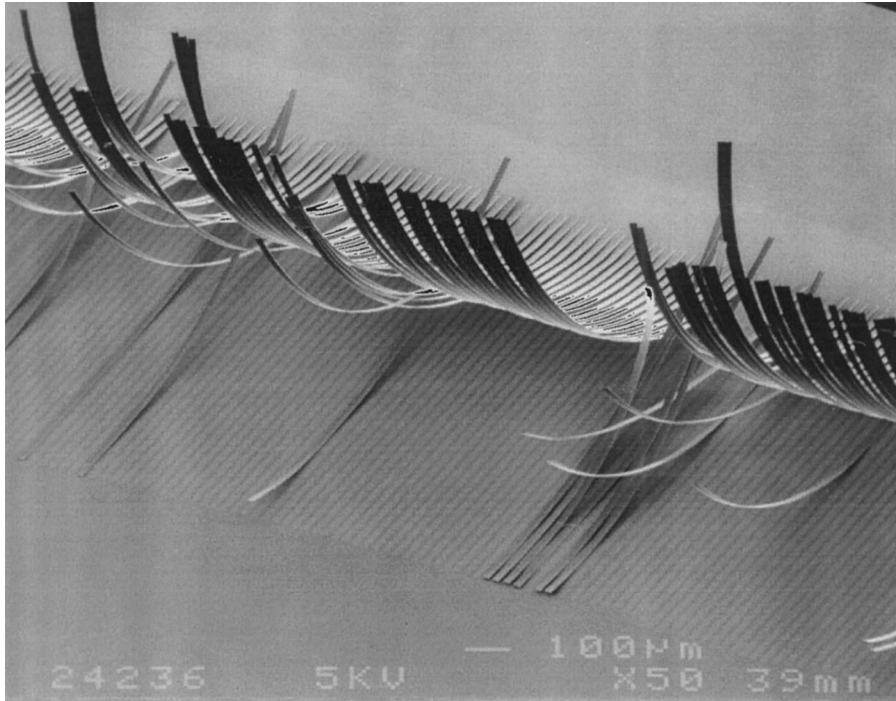
Fig. 2. A vivid illustration of the converging debond phenomenon wherein thin, residually strained strips remain attached to the substrate via small remnant ligaments.

uniform pressure p to act over the entire face area, and then p is chosen such that the opening at the center is consistent with the wedging displacement produced by the imperfection. The stress intensity factor for the cracks at A is [21]

$$K_A = p\sqrt{2b \tan \eta} \qquad (1)$$

Fig. 3. A schematic showing the displacements that arise when attached ligaments occur in association with edge delamination.

where $\eta = (\pi/2)(b - c)/b$. The associated opening at the center of the cracks is

$$\delta = \frac{8bp}{\pi \bar{E}} \cosh^{-1}[\sec \eta]. \qquad (2)$$

The energy release rate at a given opening displacement δ is obtained by eliminating p from equations (1) and (2) as

$$G_A = \frac{\pi^2}{32} \frac{\bar{E}\delta^2}{b} F_A(\eta) \qquad (3)$$

with

$$F_A(\eta) = \frac{\tan \eta}{[\cosh^{-1}(\sec \eta)]^2}.$$

The opening displacement at the center of the cracks is governed by the misfit strain, $\Delta\alpha\Delta T$ (where $\Delta\alpha$ is the thermal expansion mismatch and ΔT the temperature drop), and by the imperfection radius, R. It must have the form

$$\delta = gR\Delta\alpha\Delta T \qquad (4)$$

where g is a dimensionless coefficient of order unity which, when the ligaments are small compared with the crack spacing, depends very weakly on c/b. When equation (4) is used in equation (3), the dimensionless energy release rate is obtained as

$$\frac{G_A}{\bar{E}R(\Delta\alpha\Delta T)^2} = g^2 \frac{\pi^2}{32} \frac{R}{b} F_A(\eta). \qquad (5)$$

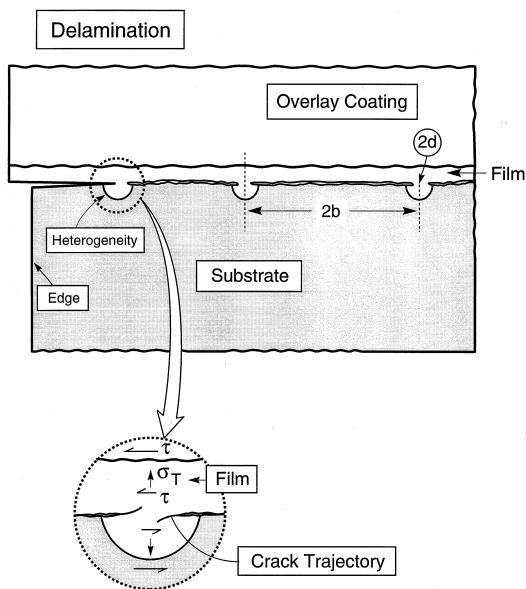The function $F_A(\eta)$ is large when c/b is near unity, decreases to a minimum, of 0.905, at $c/b = 0.18$,
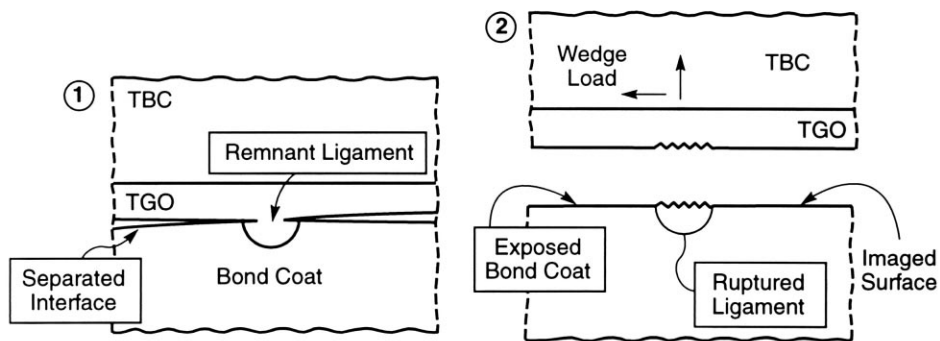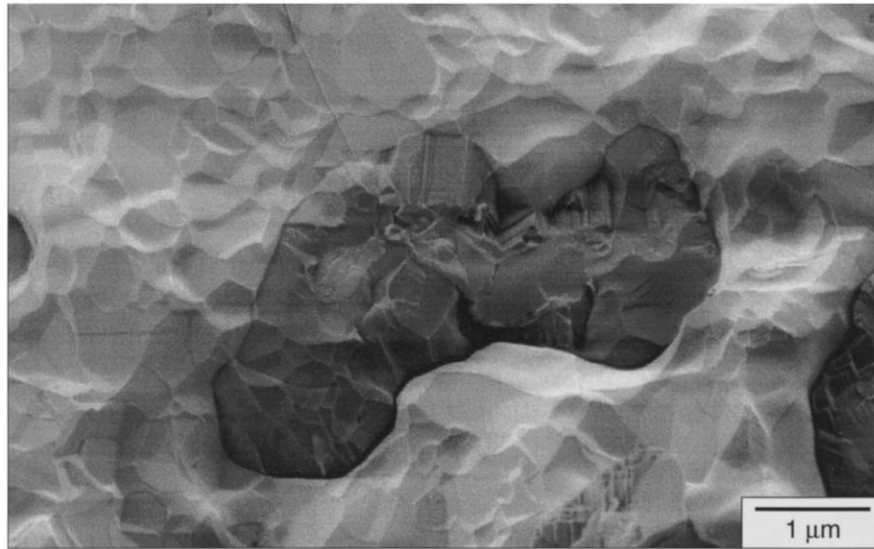
Fig. 4. A schematic showing the detachment of a TGO ligament and a scanning electron microscope image of the ruptured TGO ligament embedded in the substrate [20]. The dark contrast region is the embedded Al_2O_3.

and then increases, becoming unbounded as $c/b \longrightarrow 0$. As a consequence, separations coalesce once the ligaments have been reduced to $c/b = 0.18$. Equating $(G_A)_{minimum}$ to the fracture toughness along the weak plane, designated Γ_0, yields a criterion for coalescence of the cracks. It requires that the imperfection radius exceed a critical size, R_c, given by

$$\frac{R_c}{b} = (1.89/g)\sqrt{\frac{\Gamma_0}{\bar{E}(\Delta\alpha\Delta T)^2 b}}. \qquad (6)$$

The model result [equation (6)] is translated into a form applicable to the coalescence of the type I ligaments in a brittle film by assuming that the imperfections are spherical, radius R, and that there is one per area of interface, radius b. With f_c as the critical area fraction of these imperfections in the weak plane at coalescence, equation (6) provides

$$f_c = \xi \frac{\Gamma_0}{\bar{E}(\Delta\alpha\Delta T)^2 b} \qquad (7)$$

where ξ is a non-dimensional coefficient of order unity.

This result may be interpreted as follows. As the heterogeneities increase in size upon film growth, a critical size is reached whereupon type I separations coalesce. This event does not cause failure. Instead, a transition occurs to convergence of type II ligaments, discussed in Section 4.

In order to establish the magnitude of g, some numerical results have been obtained. For this purpose, the finite element method has been used. The method is the same as that discussed elsewhere [10, 11] for determining energy release rates. The results are shown in Fig. 5. Note that the energy release rate minimum increases with increase in R/b, as anticipated by the analytical result (5). Moreover, there is a close correspondence between the numerical and analytical results when R/b is small (≤ 0.05), such that $g \approx 1$. At larger R/b, g becomes a function of R/b. It exceeds unity and increases as R/b increases. Eventually, at $R/b \approx 0.4$, the minimum is eliminated.
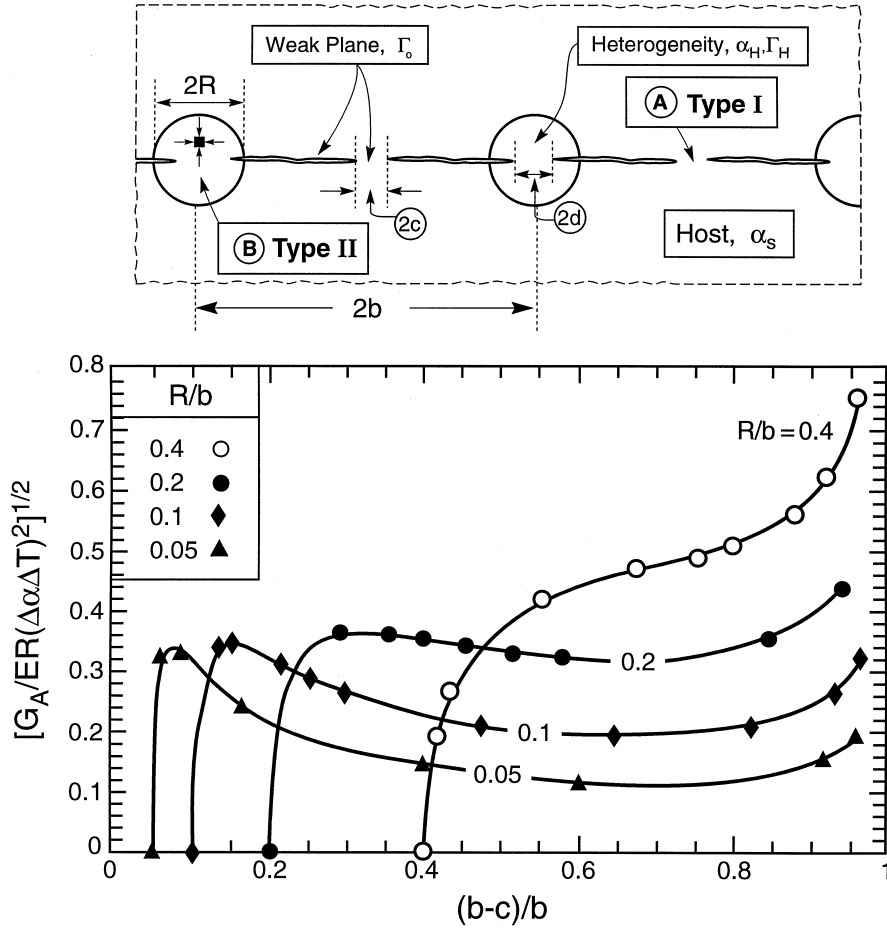
Fig. 5. Numerical results for the energy release rates at coalescing type I ligaments using the model from Fig. 1(a).

4. LIGAMENT CONVERGENCE

After the type I ligaments have failed, the coating remains attached by type II ligaments. Previous analyses of converging debonds [15–17] provide basic concepts. Namely, when the ligament radius d is small compared with the radius of the heterogeneity R, the energy release rate approaches zero as $G_B \approx \sigma_0^2 d/\bar{E}$, where σ_0 is the misfit compression in the heterogeneity, which can be related to the misfit strain $\Delta\alpha\Delta T$ in the usual way. *The residual stress is unable to fail the ligaments and the coating remains attached until some other phenomenon intervenes.* These other phenomena are examined in Section 5.

To obtain explicit results, consider an axisymmetric model of one ligament (Fig. 6), where the heterogeneity is taken to be spherical with radius R and the medium is infinitely thick. Results for the energy release rate can be derived analytically when R is small compared with the spacing ($\approx 2b$) and there is no elastic mismatch between the heterogeneity and the surrounding matrix.

For the model, take the outer radius b in the model to be infinite, and denote the radial coordinate by r. With no crack present, the misfit stress in the heterogeneity is a uniform hydrostatic pressure, $\sigma(r) = -\sigma_0$, where $\sigma_0 \equiv 2E\Delta\alpha\Delta T/[5(1-\nu)]$, while the stress acting on the incipient crack plane outside the heterogeneity ($r > R$) is tensile and given by: $\sigma(r) = \sigma_0(r/R)^{-3}$. The solution for the stress intensity factor at the tip of an external ring crack with radius d is [21]

$$K_B = \frac{2}{\sqrt{\pi d}}\int_d^\infty \sigma(r)\left[\frac{r}{d}\cos^{-1}\left(\frac{r}{d}\right) + \frac{r}{\sqrt{r^2 - d^2}}\right]dr. \quad (8)$$

The above integral can be evaluated in closed form as

$$K_B = \sigma_0\sqrt{R}\sqrt{\frac{d}{\pi R}}\left\{2\left(\frac{R}{d}\right)^3 - \left[2\left(\frac{R}{d}\right)^2\right.\right.$$
$$\left.\left. + 1\right]\sqrt{\left(\frac{R}{d}\right)^2 - 1}\right\}$$
$$\equiv \sigma_0\sqrt{R}F_B\left(\frac{d}{R}\right). \quad (9)$$

The associated energy release rate can be expressed in the dimensionless form as
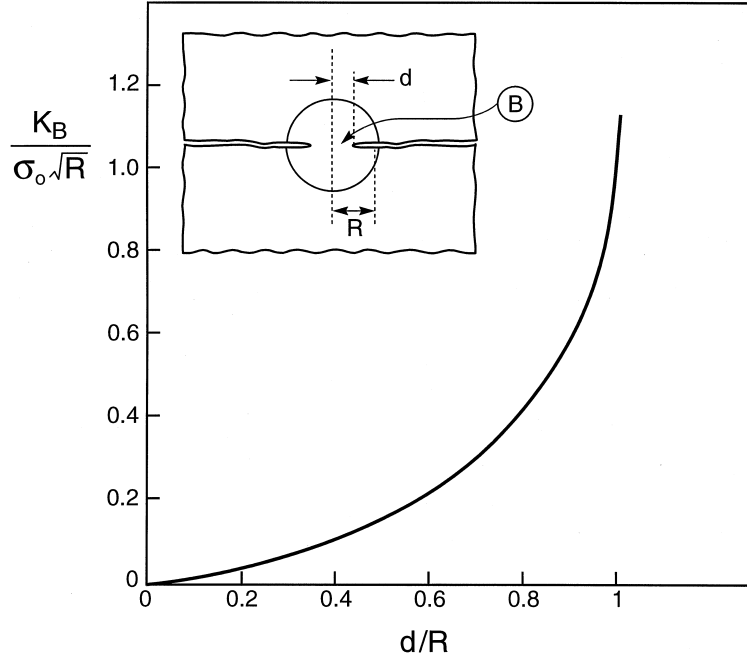
Fig. 6. Stress intensity factor for type II ligaments in the limit that the ligament size $d/b \ll 1$.

$$\frac{G_B}{E(\Delta\alpha\Delta T)^2 R} = \frac{4(1+\nu)}{25(1-\nu)}\left[F_B\left(\frac{d}{R}\right)\right]^2. \quad (10)$$

The stress intensity factor is plotted in Fig. 6. The size of the remnant ligament under the action of σ_0 can be obtained by equating K_B to the heterogeneity toughness K_{Hc}. Inserting typical values for TBCs (Table 1) to evaluate $K_{Hc}/\sigma_0\sqrt{R}$ indicates that the expected remnant ligament size is $d_*/R \approx 0.5$.

5. DETACHMENT

Several means exist whereby extra loads can arise on the attached type II ligaments causing them to fail. These include segments where the substrate has convex curvature and delaminations around edges and holes. The general role of these features is to induce forces normal (or parallel) to the ligaments, causing a change in the character of the energy release rate at the ligament. The behavior is illustrated for the model considered in the previous section when a normal load P acts across the ligament

Table 1. Properties of α-Al$_2$O$_3$ thermally grown on Ni-based bond coats

E (GPa)	380–400
ν	0.2
α_H(/°C) (p.p.m.)	7–8
α_s(/°C)^a (p.p.m.)	14–16
h (μm)	1–10
Γ_0 (J/m^2)	5–20
ΔT (°C)	1000

^{a}Ni-based superalloy.

(Fig. 7). The stress intensity factor induced by this load is [21]

$$K_B = \frac{P}{2\sqrt{\pi}d^{3/2}}. \quad (11)$$

This contribution to the stress intensity is unbounded as the ligament radius approaches zero. The combined stress intensity factor from the residual field (9) and the applied load (11) is

$$\frac{K_B}{\sigma_0\sqrt{R}} = F_B\left(\frac{d}{R}\right) + \frac{P}{\sigma_0\pi R^2}\frac{\sqrt{\pi}}{2}\left(\frac{R}{d}\right)^{3/2}. \quad (12)$$

The combined factors have a minimum at $dK_B/d(d/R) = 0$ corresponding to

$$\frac{P}{\pi\sigma_0 R^2} = \frac{2}{3\pi\beta}\left[\frac{\beta(1+2\beta^2)}{\sqrt{\beta^2-1}} + 4\beta\sqrt{\beta^2-1} - 6\beta^2\right]$$
$$- \frac{1}{3\pi\beta^2}\left[\sqrt{\beta^2-1}(1+2\beta^2) - 2\beta^3\right] \quad (13)$$

where $\beta = R/d$. Upon enforcing $K_B = K_{Hc}$ in equation (12) and then solving equations (12) and (13) simultaneously for the values, P_c and β_c, at the minimum, the results plotted in Fig. 7 are obtained. Because the stress intensity factor associated with P_c is the minimum for all d, attainment of P_c causes the ligament to undergo complete separation.

One limiting result is of interest. When the non-dimensional toughness is small,

$$P_c \approx \pi K_{Hc}^3 \sqrt{R}/\sigma_0^2. \quad (14)$$

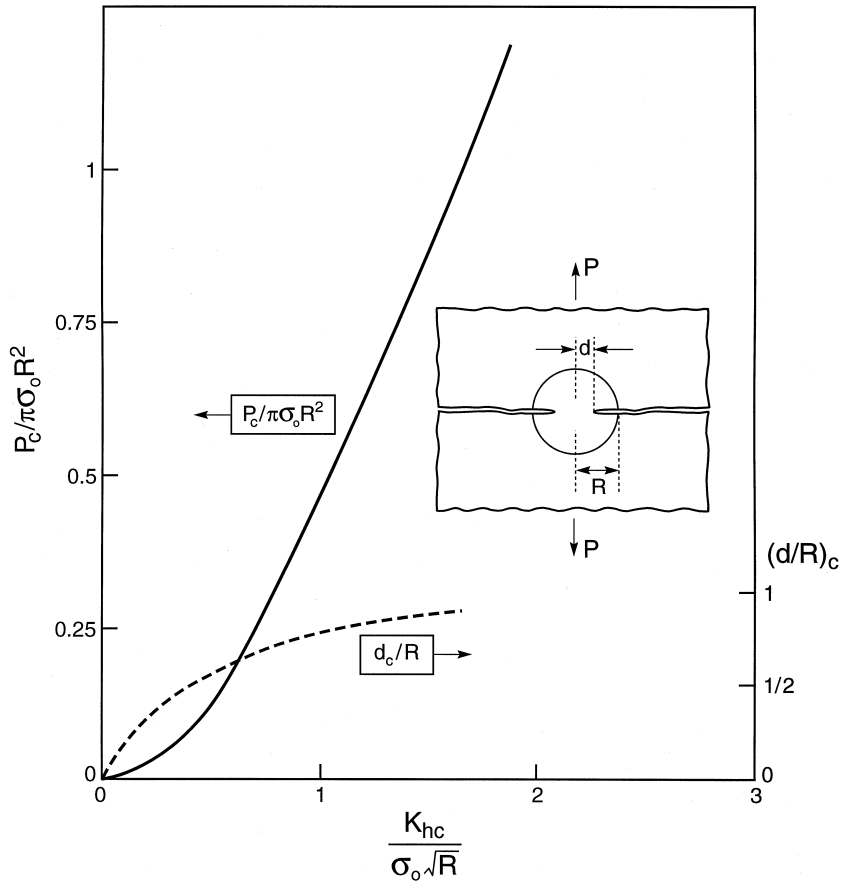Paradoxically, according to (14), coatings contain-

Fig. 7. Influence of the heterogeneity toughness on the transverse strength and critical ligament size at rupture.

ing large imperfections sustain greater loads prior to detachment. Otherwise, consistent with intuition, higher stresses and lower toughnesses are detrimental.

Introducing typical values for TBCs (Table 1), and assuming heterogeneities with $R = 10\ \mu m$ and area fraction $f \approx 0.1$ gives $\sigma_T \approx 200$ MPa. The transverse strengths are thus surprisingly large given the extensively cracked character of the system. In practice, non-periodic arrangements of remnant ligaments result in crack-like flaws that weaken the system. This issue is addressed in Section 7.

6. DETACHMENT OF FILMS

Based on the insights gained from the above analyses, numerical results are obtained for the coalescence and convergence stages of the failure of *films/coatings* [Fig. 1(b)]. The intent is to perform calculations for a typical case, primarily to verify that the basic phenomena elucidated for the model system [Fig. 1(a)] also apply to films/coatings. A more complete parametric assessment awaits further calculations. The numerical analysis has been performed for a relative heterogeneity size, $R/b = 0.2$, and for a film thickness equal to the heterogeneity
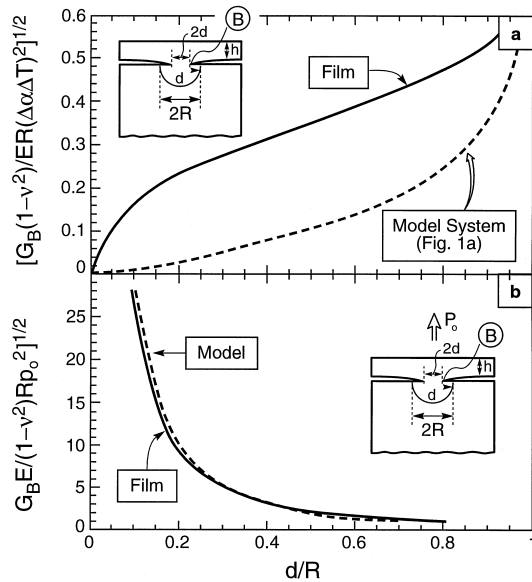

Fig. 8. Numerical results for the model depicted in Fig. 1(b), with $h/R = 1$ and $R/b = 0.2$. (a) Non-dimensional energy release rate for remnant ligament size, compared with the model system [Fig. 1(a) and Fig. 6]. (b) Energy release rate associated with detachment upon application of a transverse stress p_0.

radius, $h/R = 1$ (Fig. 8). The calculations are performed using a cylindrical cell. Two separate computations have been carried out: (i) for loading due to thermal mismatch in Fig. 8(a) and (ii) for a normal tensile stress p_0 applied directly above the inhomogeneity in Fig. 8(b). The elastic moduli are taken to be the same for the film and the substrate. The boundary conditions at the edge of the cell $(r = b)$ are taken to mimic a doubly periodic array of heterogeneities. The edge is constrained to remain straight with zero average radial stress and zero shear traction.

Results pertinent to the remnant ligament size are plotted on Fig. 8(a), which represents the rate at which the energy release rate approaches zero $G_B \longrightarrow 0$, as the ligament size, $d/R \longrightarrow 0$. Superposed on the figure is the analytical result from equation (10), previously plotted as the stress intensity factor (Fig. 6). The difference between the model result and that for the film reflects the larger energy density available in the latter, enabled by contributions from both the film and the heterogeneity. The consequence is an appreciably smaller remnant ligament size, d_*/R. For example, based on quantities relevant to a 4 μm thick thermally grown α-Al$_2$O$_3$ (Table 1), the energy release rate ordinate of Fig. 8(a) is 0.5, such that $d_*/R \approx 0.8$.

When a transverse stress, p_0, is applied [Fig. 8(b)], the associated energy release rate is almost the same as that for the model, because the free surface does not change the load transmission through the intact heterogeneity.

To assess the critical transverse stress, p_0^c, required to detach the film, denote the ordinate of the function from the numerical calculation in Fig. 8(a) by $F_T(d/r)$ and that in Fig. 8(b) by $F_p(d/r)$. Then, if each contribution to the energy release rate is approximated as mode I, the two results can be superimposed to give

$$\frac{K}{\sqrt{R}\bar{E}(\Delta\alpha\Delta T)} = F_T(d/r) + \frac{p_0}{\bar{E}(\Delta\alpha\Delta T)}F_p(d/r). \quad (15)$$

The relation between K and d/r at fixed p_0 has the same qualitative features described for the model system in Section 5. The critical detachment stress p_0^c is obtained by simultaneously minimizing K with respect to d and equating K to K_{Hc}. The result is plotted on Fig. 9. Note that the stresses are similar to those for the model problem (Fig. 7).

7. DELAMINATION AND FAILURE

If a crack is present at the interface having a radius much larger than the heterogeneity spacing, the fracture toughness controls the transverse strength and the delamination resistance. In mode I loading, wherein the separations converge in a coplanar manner, the toughness is governed simply by the ligament area fraction and the heterogeneity toughness, Γ_H. This must be the case, since the process is strictly elastic and stable [22]. Thus, in
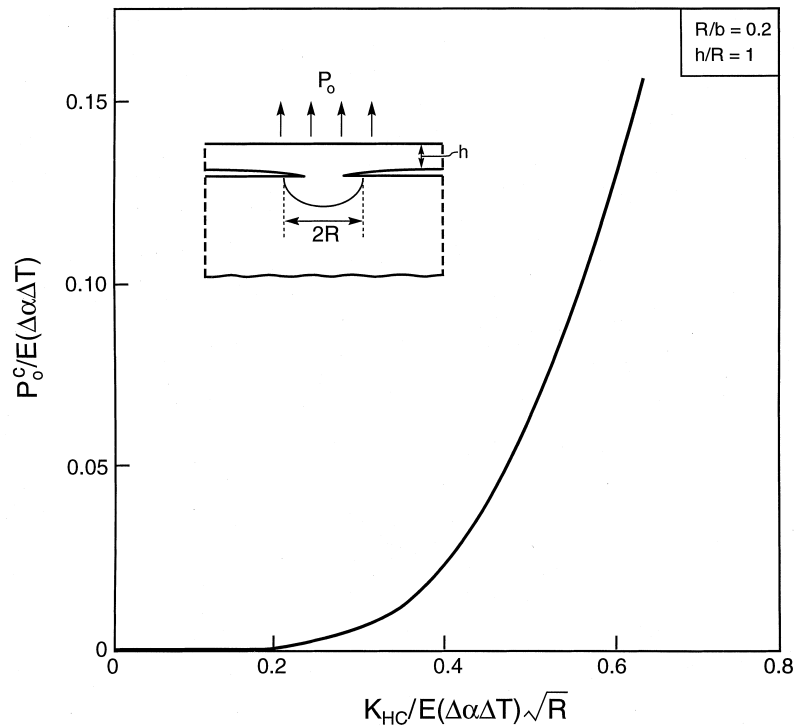

Fig. 9. Critical detachment stress for a film on a substrate [Fig. 1(b)], determined from the numerical results of Fig. 8.

steady-state, the toughness is

$$\Gamma_{ss} = (d_*/b)^2 \Gamma_H \qquad (16)$$

where d_* is obtained from equation (10) with $G_B = \Gamma_H$. Inserting typical values for TBCs indicates that $\Gamma_{ss} \approx 0.1\,\mathrm{J/m^2}$. Such a low toughness would cause inferior TBC durability, whenever areas subject to mode I loading are present. However, this constitutes a lower bound, since mode I situations are rarely encountered in residually compressed coatings.

More generally, interface cracks experience mixed mode loadings. For example, edge delaminations (Fig. 3) are subject to pure mode II with associated friction [22]. A component of mode II loading changes the ligament detachment mechanism, as sketched on Fig. 3. The key feature is that the mode mixity causes the cracks in the ligament to *diverge* rather than converge. The eventual failure of the ligaments requires a curved coalescence trajectory resulting in frictional contacts. The latter can substantially enhance the toughness, but predictions are not yet tractable.

8. SUMMARY

The major finding of the present analysis is that residually compressed films and coatings can have high durability because of the existence of remnant ligaments that arise as a natural consequence of the mechanics of residually stressed systems. These ligaments are particularly durable when the heterogeneity sites that initiate interface decohesion are distributed periodically along the surface. In this case, detachment of the film/coating requires application of appreciable transverse tensions, of order 100 MPa. Such stresses can arise in regions of high convexity and in situations that induce mechanical loads. When the heterogeneities are stochastically dispersed along the interface and, when well-defined edge delaminations exist (such as at edges or holes), the durability is substantially reduced. While the actual integrity of the coating has yet to be explicitly analyzed, a lower bound has been established by determining the mode I fracture toughness of the remnant ligaments. It is only of order $0.1\,\mathrm{J/m^2}$,

such that the transverse strength is only a few MPa when flaws of order 50 μm are present. In practice, the durability will be greater, because it is much more difficult to fail the remnant ligament when the loading is predominantly mode II, which it is for edge delaminations. Further measurements and analysis are needed to understand the delamination strength.

REFERENCES

1. Miller, R. A., *J. Thermal Spray Technol.*, 1997, **6**, 35.
2. Cross, L. A., Stewart, S. F. and Ortiz, M., *J. Engng Gas Turbines Pwr*, 1988, **110**, 610.
3. Brindley, W. J. and Miller, R. A., *Surf. Coat. Technol.*, 1990, **43/44**, 446.
4. Taylor, T. A., Appleby, D. L., Weatherill, A. E. and Griffiths, J., *Surf. Coat. Technol.*, 1990, **43/44**, 470.
5. Miller, R. A., *J. Am. Ceram. Soc.*, 1984, **67**, 517.
6. Christensen, R. J., Tolpygo, V. K. and Clarke, D. R., *Acta mater.*, 1997, **45**, 1761.
7. Tolpygo, V. K., Dryden, J. R. and Clarke, D. R., *Acta mater.*, 1998, **46**, 927.
8. Stasik, M. C., Pettit, F. S., Meier, G. H., Ashary, A. and Smialek, J. L., *Scripta metall. mater.*, 1994, **31**, 1645.
9. Scott, F. H. and Atkinson, A., *Mater. High Temp.*, 1994, **12**, 195.
10. He, M. Y., Evans, A. G. and Hutchinson, J. W., *Mater Sci. Engng*, 1998, **A245**, 168.
11. Evans, A. G., He, M. Y. and Hutchinson, J. W., *Acta mater.*, 1997, **45**, 3543.
12. Topylgo, V. K. and Clarke, D. R., *Acta mater.*, 1998, **46**, 5167.
13. Choi, S. R., Hutchinson, J. W. and Evans, A. G., *Mech. Mater.*, submitted.
14. Gioia, G. and Ortiz, M., *Adv. Appl. Mech.*, 1997, **33**, 120.
15. Hutchinson, J. W. and Jensen, H. M., *Mech. Mater.*, 1990, **9**, 139.
16. Zhuk, A., Evans, A. G., Hutchinson, J. W. and Whitesides, G. M., *J. Mater. Res.*, 1998, **13**, 3555.
17. He, M. Y., Evans, A. G. and Hutchinson, J. W., *Acta mater.*, 1997, **45**, 3481.
18. Marshall, D. B., Lawn, B. R. and Evans, A. G., *J. Am. Ceram. Soc.*, 1982, **65**, 561.
19. Evans, A. G., McMeeking, R. M., Charalambides, P. G. and Hutchinson, J. W., *Acta metall.*, 1987, **35**, 2701.
20. Mumm, D. R. and Evans, A. G., to be published.
21. Tada, H., Paris, P. and Irwin, G., *Handbook of Stress Intensity Factors.* Dell Research, 1985.
22. He, M. Y., Wissuchek, D. J. and Evans, A. G., *Acta mater.*, 1997, **45**, 2813.